JOURNAL OF ENGINEERING SCIENCES

Volume 11, Issue 1 (2024)

Salenko O., Drahobetskyi V., Symonova A., Onishchenko E., Kostenko A., Tsurkan D., Vasiukov D. (2024). Damage behavior of multilayer axisymmetric shells obtained by the FDM method. Journal of Engineering Sciences (Ukraine), Vol. 11(1), pp. D27–D35. https://doi.org/10.21272/jes.2024.11(1).d4

Damage Behavior of Multilayer Axisymmetric Shells Obtained by the FDM Method

Salenko O.[1][0000-0002-5685-6225], Drahobetskyi V.[2*][0000-0001-9637-3079], Symonova A.[2][0000-0003-1411-6656], Onishchenko E.[1][0000-0002-7600-3668], Kostenko A.[1][0000-0003-3350-5323], Tsurkan D.[1][0000-0002-4240-6231], Vasiukov D.[3][0000-0002-1010-4191]

[1] National Technical University of Ukraine “Igor Sikorsky Kyiv Polytechnic Institute”, 37, Peremohy Ave., Kyiv, 03056 Ukraine;
[2] Kremenchuk Mykhailo Ostrohradskyi National University, 20, Pershotravneva St., 39600 Kremenchuk, Ukraine;
[3] IMT Nord Europe, École Mines Télécom, IMT-Université de Lille, Guglielmo Marconi St., F-59650 Villeneuve-d’Ascq, France

Article info:

Submitted:	September 4, 2023
Received in revised form:	December 27, 2023
Accepted for publication:	January 2, 2024
Available online:	January 11, 2024

***Corresponding email:**
vldrag@kdu.edu.ua

Abstract. This research rigorously explores the additive synthesis of structural components, focusing on unraveling the challenges and defect mechanisms intrinsic to the fused deposition modeling (FDM) process. Leveraging a comprehensive literature review and employing theoretical modeling and finite element analysis using ANSYS software, the study meticulously investigates the behavior of multilayer axisymmetric shells under varying internal pressure conditions. Critical parameters are identified, and the impact of design factors, including material properties, geometric parameters, and internal pressure, is quantitatively assessed using a rich digital dataset. In a series of model experiments, the study reveals specific numerical results that underscore the progressive nature of damage development in FDM-produced multilayer axisymmetric shells. Notably, under increasing internal pressure, stresses on the tank’s inner walls reach up to 27.5 MPa, emphasizing the critical importance of considering material properties in the design phase. The research also uncovers that the thickness of tank walls, while significant in resulting stresses, does not markedly impact the damage development mechanism. However, it places a premium on selecting rational parameters for the honeycomb system, including shell thickness, honeycomb height, honeycomb wall thickness, and honeycomb cell size, to minimize stress concentrations and enhance structural integrity. The inclusion of honeycomb structures in the tank design, as evidenced by specific results, provides enhanced thermal insulation properties. The research demonstrates that this design feature helps localize damage and mitigates the formation of significant trunk cracks, particularly along generative cracks.

Keywords: additive synthesis, honeycomb structures, damage development, finite element analysis.

1 Introduction

The techniques for additive synthesis of prototypes, mock-ups, and structural components represent a highly promising avenue within the field of forming [1]. This approach holds significant potential for realizing “smart production,” focused on creating entirely novel products, materials, and workpieces while minimizing raw material usage and maximizing equipment standardization. Despite ongoing worldwide research efforts to explore the applications of additive technologies, these processes remain insufficiently understood. Nevertheless, the expansive prospects for industrial production in this domain motivate scientists to redouble their endeavors, seeking innovative methods, techniques, and materials conducive to effectively implementing these technologies.

Concurrently, the proliferation of additive technologies in engineering practice encounters specific challenges. Primarily, these hurdles stem from the limited reliability of the process and the need for consistent reproducibility when fabricating parts and components subject to stringent requirements concerning density, geometric precision, mechanical strength, and surface layer attributes. From this perspective, identifying the causative factors and underlying mechanisms responsible for defects in components produced via the Fused Deposition Modeling (FDM) process is essential for devising efficient means to enhance their quality.

This matter is significant in producing thin-walled or honeycomb structures that withstand thermobaric loads. Typical instances of such structures include tanks employed for diverse technological applications, such as medical oxygen storage or aerospace fuel containment [2]. These systems demand rigorous technical specifications and high reliability, necessitating a predictive understanding of the synthesis outcomes. Consequently, investigating damage patterns in multilayer axisymmetric shells produced via the FDM method has emerged as a crucial and active research area.

2 Literature Review

A substantial body of literature delineates the core principles of additive synthesis methods. Notably, work [3] explains the basic concepts of additive manufacturing (AM) and describes the process from design to applications. The layer formation process and the overall product constitution are described in [4].

Certain publications, exemplified by [5], supply data regarding the strength characteristics of both samples, allowing the evaluation of material properties post-extrusion and the attributes of the final products [6]. Some research endeavors, for instance, [7], endeavor to amalgamate insights into the fracture patterns of examined samples through cross-sectional analyses resulting from critical mechanical loads. In a separate study [8], the authors systematically categorize the origins of various defect types arising from both intrinsic system factors and external influences. These authors construct a failure frequency histogram gleaned from the sustained operation of FDM printers.

Explorations into spatial and form errors in components produced through the filament deposition of materials such as ABS, PLA, CoPET, and select high-temperature plastics are noted in [9]. The findings of this study culminated in the conclusion that thermal errors, denoted as δ, are directly contingent upon factors encompassing the mass of extruded plastic, its volume within specific elements of the product, and external variables (e. g., temperature gradients on the work surface). The authors also posit that using “sacrificial elements” is advisable to mitigate δ and residual stress ($\sigma 0$), thereby averting product deformation.

Finite element analysis (FEA) is prevalent for modeling damage evolution in FDM-manufactured shells under mechanical loading conditions. An investigation detailed by Caminero et al. [10] conducted a numerical study using FEA to investigate damage development in FDM-printed multilayer shells under impact loading. The study revealed that delamination and interlamellar cracks were the main types of damage observed, and the critical energy release rate was identified as a key parameter for predicting delamination onset and propagation.

Another approach is cohesive zone modeling, which represents delamination behavior as cohesive interfaces with defined failure parameters. The work [11] developed a cohesive zone model to simulate damage evolution in FDM multilayer axisymmetric shells under tensile loading. The model, calibrated with experimental characterization, successfully captured peel behavior and exhibited good agreement with experimental observations, providing insight into damage progression and failure mechanisms.

Further research [12] substantiates the direct relationship between the mechanical properties and damage susceptibility of FDM-printed shells with layer thickness and interlayer bonding. Thicker layers and inadequate interlayer cohesion are shown to diminish strength, amplify delamination, and compromise overall structural integrity. Moreover, the orientation of printed layers relative to the loading direction significantly influences the shells’ strength, rigidity, and failure modes. FDM’s layer-wise deposition process introduces anisotropic traits impacting mechanical properties and damage behavior.

Work [13] presents outcomes about the stress-deformation state of honeycomb systems, accentuating the importance of continued research and prospects within industrial applications of these technologies. Meanwhile, a detailed exposition of multilayer shell structure manufacturing and associated calculations is presented in [14], delineating particular shell product behavior in [15].

In theoretical analysis concerning the shape change and deformation of sheet components and workpieces, particularly under pulsed and static loading, numerical methods and standard software packages are deemed most suitable [16]. The fundamental principle of the finite element method involves dividing the studied area into cells using families of coordinate lines. Nodes, categorized into internal and boundary points, are formed at the intersection of these coordinate lines. The method replaces the required function with a set of values at these nodal points, reducing the problem of solving a system of linear algebraic equations and determining the numerical values of the desired function at the nodes [17].

However, challenges arise when calculating deformation processes in layered plates and shells through finite element methods. These challenges stem from difficulties in aligning elements with models of homogeneous layers and a notable increase in interlayer stresses in the edge effect zone.

To accurately predict the performance of composite materials and understand the impact of structural, compositional, and technological parameters, developing a comprehensive theory that addresses control at all stages of production and operation becomes imperative.

The processing technologies for layered compositions present unique challenges. The metals constituting multilayer metal compositions exhibit diverse physical and mechanical properties, distinct chemical compositions, and varied micro- and macrostructures. These inherent differences necessitate careful consideration when devising technological processes for processing layered compositions. Whether the layered composition comprises homogeneous materials significantly influences and adjusts the processing technology involved.

The current research lacks a comprehensive understanding of the mechanisms causing defects in FDM-manufactured structural components. Identifying these mechanisms and their impact on structural integrity remains an unexplored aspect. Also, a research gap exists in predicting damage patterns in thin-walled structures subjected to thermobaric loads, specifically in multilayer axisymmetric shells produced via the FDM method.

This work aims to fill research gaps related to defect mechanisms, reliability challenges, and predictive understanding of damage in thin-walled structures under thermobaric loads.

Among the goals of the research, we should highlight the study of the progressive development of damage in multilayer axisymmetric shells produced via FDM under thermobaric loads and the quantitative determination of design parameters, including shell thickness, honeycomb features, and material properties, on stress concentrations. Through these objectives, the research seeks to provide actionable insights for advancing additive manufacturing processes, ensuring the production of structurally sound components with enhanced reliability.

3 Research Methodology

3.1 Theoretical fundamentals of modeling

We consider the product as a layered shell with interlayers of discrete materials to perform verification calculations of the structure. This shell, in the process of deformation, is described by a limited multiply connected surface, has isotropic or aniso-tropic properties in the direction of the deformation axes, and is described by a surface or a system of surfaces (solid and discrete) of a canonical form:

$$x_3 = S(x_1, x_2, t), \quad (1)$$

where x_1, x_2, and x_3 – workpiece coordinates in the reference system (x_0, x_1, x_2, x_3); t – time.

We consider that the surface S is bounded by a system of internal simple contours L_i (i =1, 2, …, n) and contour $L_{(n+1)}$ that encloses internal contours L_i.

The shell has a system m of arbitrarily oriented intersecting reinforcing elements bounded by contours Ri (i = 1, 2, …, m).

The deformed state looks like this:

$$\varepsilon_j = \varepsilon_j(x_1, x_2). \quad (2)$$

When addressing the nonlinear deformation of shells, including nonlinear elastic, viscoelastic, or viscoplastic behavior (using a generalized Maxwell model with variable viscosity coefficients), the shell's middle surface is associated with a spatial Lagrange's grid, denoted as X^1X^2. In this approach, the quantities within the shell are determined based on the quantities at the corresponding nodal points.

For the inclusion of reinforcing elements, local coordinate systems x_i^m are introduced, and the coordinates of the intersection centers of the reinforcing discrete shell are denoted as O_n.

During the modeling of nonlinear elastic deformation of the shell, the shell's surface is treated as a continuous flat surface, considering that the shell is forming a bounded, multiply-connected surface. The solid shell represents a bounded and connected region where internal stress sources or sinks are concentrated along the contours corresponding to reinforcing elements (such as honeycombs). This leads to discontinuities in displacements and rotation angles. The components of deformation resulting from these stress sources and sinks are expressed using functionals concentrated on the contours, combining the displacement jumps and rotation angles within the resolving differential equations. By employing an integral representation of the solution to these equations while satisfying the boundary conditions along the contours of the reinforcing shell, the problem can be reduced to a system of singular integral equations to determine the desired densities. In some instances, the solution to these integral equations can be obtained analytically in the form of series expansion with respect to a small parameter. Analytical solutions are feasible when the local reinforcing elements have simple contours (rectangles, hexagons, circles, and ellipses).

To determine the loads acting on the grid nodes and elements, the equation of motion is written in the tensor notation for brevity and convenience.

$$\nabla_\beta H_{mn}^{\beta\alpha} - Q_{mn}^{\beta} B_{\beta_{mn}}^{\beta} + F_{mn}^{\alpha} + Z_{mn}^{\alpha} + I_{mn}^{\alpha} = 0; \quad (3)$$

$$H_{mn}^{\beta\alpha} B_{\beta\alpha}^{mn} + \nabla_\beta Q_{\beta}^{mn} + F_{mn}^{3} + Z_{mn}^{3} + I_{mn}^{3} = 0, \quad (4)$$

where $H_{mn}^{\beta\alpha}$ – membrane forces; Q_{mn}^{β} – cutting forces; $B_{\beta_{mn}}^{\beta}$ – curvature tensor; ∇_β – a sign of covariant differentiation; F_{mn}^{α} – force applied to the shell; Z_{mn}^{α} – interlayer friction forces; I_{mn}^{α} – forces acting on the workpiece from the reinforcing elements' flanges.

We supplement equations (3/1) with the moment equations

$$\nabla_\beta L_{mn}^{\alpha\beta} - Q_{mn}^{\alpha} = 0 \quad (5)$$

and physical law:

$$w(\sigma_{\alpha\beta}^{mn}, \varepsilon_{\alpha\beta}^{mn}, \dot{\varepsilon}_{\alpha\beta}^{mn}) = 0. \quad (6)$$

The pressure F_{mn}^{j} – related to the unit area of the shell surface and acts in the direction of the normal N_{mn}^{j}. In the calculations, we restrict ourselves to the case of an edge load (the design case of the formation of relief elements, the model of rigid pinching). A force vector is assumed to act along a particular boundary curve, a unit length of the undeformed middle surface.

The determination of each node's position on the middle surface of the workpiece is achieved through the "forced displacement" diagram. The basis vectors (covariant basis) are determined at each node of the computational grid.

The increment of the metric curvature tensor is considered to calculate the components of the strain tensor. It is assumed that the shell being studied is thin, a natural assumption for this class of components.

A multilayer model with sublayers is utilized to calculate shell deformations. Research [18] has shown that using four layers based on the shell's thickness is optimal. Each layer of the shell is assumed to consist of four sublayers of equal thickness, where the material is concentrated, and these sublayers operate under conditions of a plane stress state. The layers are equidistant from each other and are separated by a material that cannot sustain a plane stress state in the tangent plane of the shell but possesses infinitely high shear transverse rigidity.

In the problem, stresses and their increments are determined by the strain increments in each node and layer of the shell being studied. The strain tensor increment is decomposed into elastic, viscous, and plastic components:

$$\Delta\varepsilon_{\alpha\beta}^{mn} = \Delta\varepsilon_{\alpha\beta}^{mn,Y} + \varepsilon_{\alpha\beta}^{mn,\Pi} + \varepsilon_{\alpha\beta}^{mn,V} = 0. \quad (7)$$

The elastic components of the strain increment tensor are determined by employing the mechanical equation of state, considering a variable shear modulus. In this case, the relationship between stress and strain deviators exhibits nonlinear behavior. The mechanical process of composite destruction is divided into two stages. The first is scattered destruction, which involves initiating a system of microcracks and developing main cracks. A specialized local fractures theory describes the development of cracks.

When interlayers of dispersed materials are present, the differential equations governing the dynamic equilibrium of the element take the form (4). The strain increments can be expressed as follows:

$$\Delta\varepsilon_{\gamma,\eta,\tau}^{k,l,m} = (\Delta\varepsilon_{\gamma,\eta,\tau}^{k,l,m})^p - \left(\Delta\varepsilon_{\gamma,\eta,\tau}^{k,l,m}\right)^t; \quad (8)$$

$$(\Delta\varepsilon_{\gamma,\eta,\tau}^{k,l,m})^p = \Delta\lambda_{\gamma,\eta,\tau}\sigma_{\gamma,\eta,\tau}^{k,l,m}, \quad (9)$$

where $\varepsilon_{\gamma,\eta,\tau}^{k,l,m}$ – strain deviator components, $\sigma_{\gamma,\eta,\tau}^{k,l,m}$ – stress deviator components, $\Delta\lambda_{\gamma,\eta,\tau}$ – measure of plastic deformation, k,l – indices; γ – node number, η – layer number; τ – time point of the deformation process.

The relationship equation between strain rates and stresses, as well as kinematic relations and the continuity equation, have the form:

$$\sigma_{ik} = \frac{\tau_s}{\sqrt{f_1^2 H^2 + f_2^2 \xi_\theta}}\left[f_1\xi_{ik} + \left(f_2 - \frac{1}{3}f_1\right)\delta_{ik}\xi_0\right]; \quad (10)$$

$$\xi_{ik} = \frac{1}{2}\left(\dot{\varepsilon_{i,k}} + \dot{\varepsilon_{k,i}}\right); \quad (11)$$

$$\frac{\partial\rho}{\partial t} + \frac{\rho_{i,i}\cdot\dot{\varepsilon}_i}{\rho} + \xi_0 = 0, \quad (12)$$

where σ_{ik} and ξ_{ik} – stress and strain rate tensors; $\dot{\varepsilon}_i$ – velocity vector; $\xi_\theta = \xi_i$ – a rate of volumetric changes; τ_s – deformation resistance of the base material; H – strain rate intensity; ρ – relative density; f_1, f_2 – functions of ρ included in the plasticity condition of the ellipsoidal type, related by the equation.

$$\frac{T^2}{f_1^2} + \frac{\sigma_0^2}{f_2^2} = 1, \quad (13)$$

where T – the intensity of shear stresses; σ_0 – average voltage.

The physical law (rheological equation) is taken as

$$T = T(\rho_0, \Lambda, \varepsilon); \;\; \sigma = \sigma(\rho_0, \Lambda, \varepsilon). \quad (14)$$

The presence of cavities and defects in the printed product and their influence on the physical and mechanical properties were considered based on the determination of the stress intensity factor (SIF) for nucleated and undeveloped cracks. Their density can be established based on mechanical tests of samples. The method of calculating SIF is obtained from [18], according to which the values of K_I based on energy methods for determining the J-integral are:

$$K_I = \sigma\sqrt{\pi l}\,\frac{1+k-(1-k)\cos 2\beta}{2}; \quad (15)$$

$$K_{II} = \sigma\sqrt{\pi l}\,\frac{1-k}{2}\sin 2\beta, \quad (16)$$

where k =1 under the condition of a flat stress state; $k = 1 - v^2$ – under the condition of plane deformation; $2l$ – width of the crack; $2b$ – width of the sample; β – angle between the crack plane and the equivalent load.

Since the filament went through the stages of melting, extrusion, laying, and solidification before forming the product, the phenomena that occurred before the cooling of the finished product were also considered.

For the melt of the filament (polymer thread), the tangential stresses τ are set according to [19] as follows:

$$\tau = K_{1e}^{-\beta\frac{T-T_1}{T_1-273}}\dot{\gamma^n}, \quad (17)$$

where β – temperature coefficient; K – consistency coefficient (effective viscosity), γ – tangential stress.

Flow curve for polymer melt:

$$\tau = K\dot{\gamma^n}, \quad (18)$$

where n is an exponent that characterizes the degree of non-Newtonian melt behavior and is the flow index.

The coefficient K is a function of temperature $Ke^{-\beta}$:

$$\beta = -\frac{T_1}{(T_2 - T_1)}\ln\left(\frac{K_2}{K_1}\right)Ke^{-\beta}. \quad (19)$$

The least squares method determined the rheological parameters K and n according to experimental data [18].

The developed mathematical model is a valuable tool for incorporating the distinctive properties and structural characteristics of materials produced through the FDM method. Notably, the model accounts for the intricacies of material behavior post-extrusion, considering factors such as nonlinear deformation, viscoelasticity, and voids or looseness in the material.

In particular, the model allows for considering material properties after extrusion through the nozzle, offering a realistic representation of the conditions encountered during the additive manufacturing process. This includes accounting for phenomena such as melting, extrusion, laying, and solidification stages, which collectively influence the final properties of the fabricated product.

By integrating these aspects into the FEM simulations, the mathematical model facilitates model experiments that closely align with real-world scenarios. The inclusion of material-specific properties and the acknowledgment of looseness in the material contribute to the fidelity of the simulations, allowing for a more nuanced understanding of how the material behaves under various conditions.

3.2 Finite element analysis

The research involved conducting virtual experiments using the ANSYS software environment. This enabled the solution of various stationary and non-stationary spatial problems related to the mechanics of deformed solid bodies. These included problems of non-stationary geometrically and physically nonlinear contact interactions between structural elements, fluid and gas mechanics, heat transfer, heat exchange, electrodynamics, and acoustics, as well as the mechanics of plowed fields. Statistical data processing and experiment planning were carried out using StatGraphics, facilitating experiment planning, statistical analysis, and the derivation of regression equations for the investigated processes and systems.

Two tank models were developed to facilitate the research. The first model was a spherical tank with a nipple for supplying the working medium, which consisted of two walls with honeycomb filling (Fig. 1a). The second model was a cylindrical tank with two flanges, designed similarly to the spherical tank (Fig. 1b).

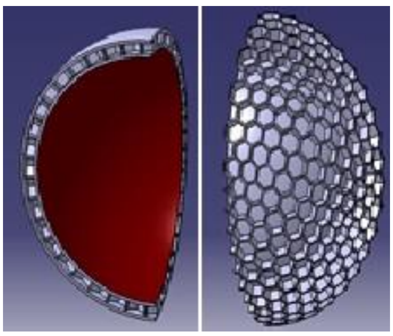

a

b

Figure 1 – Model of spherical (a) and cylindrical (b) tanks

Including honeycomb filling in the tank design allowed for connecting two concentric shells while ensuring high thermal insulation properties.

The research was conducted in two stages. In the first stage, the influence of the geometric parameters of the shell on the stresses within the walls was investigated. In the second stage, the dynamics of shell damage were evaluated under various laying conditions, including the effect of self-bonding. The tested tank was subjected to loading until it reached the point of deformation or destruction.

Theoretical studies were performed using generated solid-state models. Sixteen models with the same inner radius of 115 mm were created for calculations. The thickness of the shell walls, the size of the honeycomb cells, the honeycomb height, and the honeycomb walls' thickness varied depending on the experimental conditions. The models were initially created using CATIA v.5 and then imported into ANSYS in *.step format. The constructive implementation of the tank is illustrated in Figure 2.

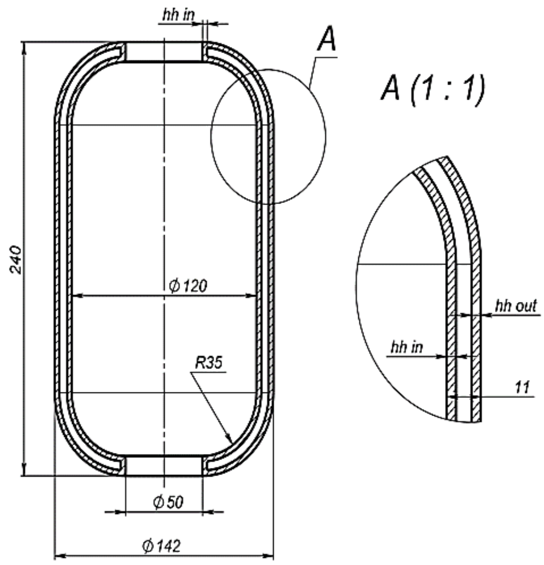

Figure 2 – Constructive implementation of the tank

The body of the product and its properties during mathematical modeling of the behavior of the shell under the action of the internal load until the moment of destruction is given in Table 1.

Table 1 – Material properties

Properties of PC		Components
Model type	linear, spring, isotropic	Solid-body 1 (cylindrical tank)
Standard strength criterion	–	
Tensile strength limit, N/m²	$3 \cdot 10^7$	
Modulus of elasticity, N/m²	$2 \cdot 10^9$	
Shear modulus, N/m²	$3.19 \cdot 10^8$	
Poisson's ratio	0.394	
Density, kg/m³	1020	

When preparing the model, the mesh type was chosen as a standard mesh on a solid body. The detailed characteristics of the mesh are as follows: total nodes – $9.65 \cdot 10^4$; total elements – $6.02 \cdot 10^4$; maximum aspect ratio – 20.3; percentage of elements with aspect ratio less than 3 – 97.4 %, percentage of elements with aspect ratio less than 10 – 0.18 %; percentage of distorted elements – 0 %. Overall, the quality grid is defined as high.

The self-bonding process was modeled by changing the temperature T_0 in the printer chamber after laying the first (base) layer and by changing the extrusion conditions. The simulation results were compared with a full-scale experiment that estimated the tank shells' stresses.

Variable parameters were also the following: tank shell thickness (x_1), honeycomb height (x_2), honeycomb wall thickness (x_3), and honeycomb cell size (x_4). The choice of these parameters was due to the search for rational design parameters of the tank while minimizing the weight (at the maximum p_{max}, and therefore $[\sigma]$ of the product). Self-bonding was performed by changing the extrusion conditions. It was believed that the stresses were formed during the solidification of the outer layer from the temperature Tl=210^{0}C to the base temperature (T_0 = 20 °C), which took place within 12 minutes will allow for forming residual stresses in the layer at the level of 15–18 MPa. Simultaneously, the maximum expected stresses before failure should be 28–32 MPa.

4 Results

At the first research stage, the shell itself was imagined as anisotropic, the material of which is quasi-elastic with a limited area of plasticity. This made it possible to establish the distribution of stresses (normal and tangential) along the section of the shell wall. Since the load from liquid or gas applied to the inner wall was p_b = 0.5 MPa in the calculations, no significant deformations or damages were detected. A further increase in the load p_b begins to cause a sharp increase in stresses, with a simultaneous reduction in the margin of strength, Figure 3.

The central part of the product experiences the maximum deformation, and it is there that the destruction of the sample occurs (Figure 4).

Comparison of the simulation results with the full-scale test of the tank demonstrator before destruction, Fig. 4b proves an almost identical picture. However, the experiment showed only interlayer destruction of the demonstrator.

The dynamics of tank destruction are progressive, and as the load increases, the deformation increases like an avalanche. This is because the damage formed on the internal defects can be combined within a particular area, with a simultaneous drop in the resistance to destruction and the release of energy when considering the investigated body as quasi-brittle. Therefore, the loss of working capacity corresponds to the model we described in [20].

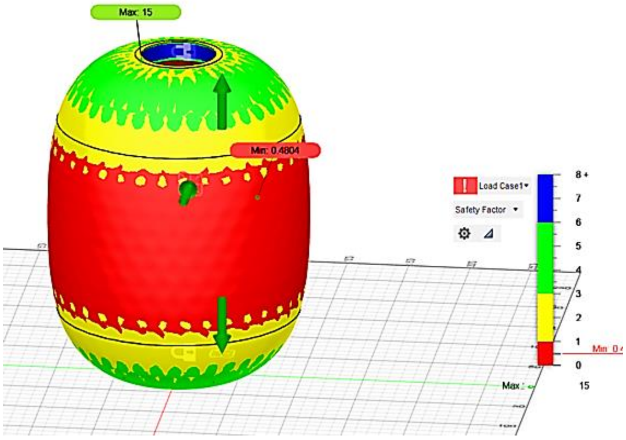

a

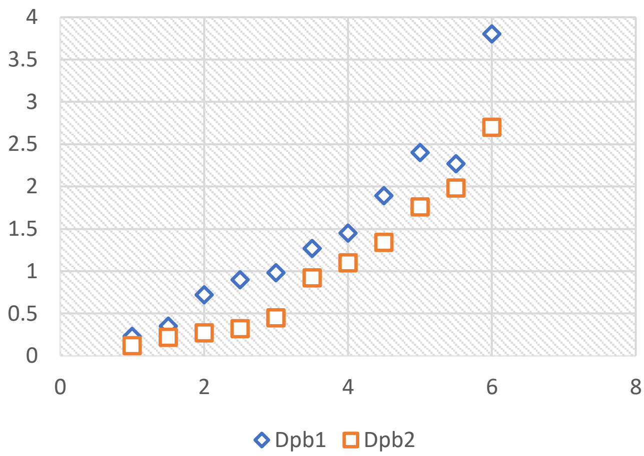

b

Figure 3 – The change in strength reserves when the internal pressure increases tank of the demonstrator (a) and deformation of the tank (b) for different dynamics pressure changes: Δp_{b1} = 0.1 MPa/s; Δp_{b2} = 0.02 MPa/s

a

b

Figure 4 – Damage (destruction) of the balloon: a – simulation results; b – experimental results

Simultaneously, damage to the shell (tank) will occur in the middle section; the presence of an intermediate honeycomb does not cause the appearance of significant trunk cracks (in particular, along the generative cracks) but localizes the damage in areas where the specific density of defects is the greatest.

The calculations also showed that the thickness of the tank walls does not significantly affect the damage development mechanism, although the changes in the resulting stresses are significant (Figure 5).

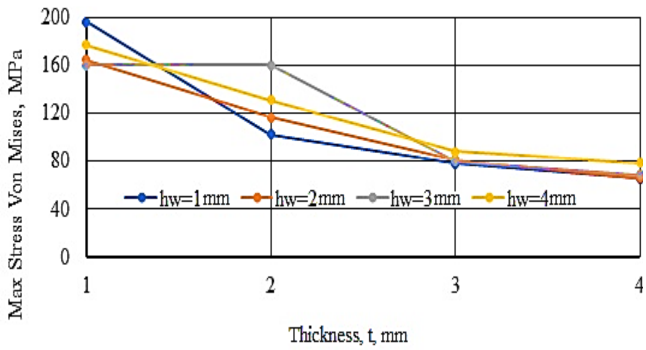

Figure 5 – Change in maximum stresses under the influence of p_b for different thicknesses of the honeycomb and tank walls

It can be stated that the considered model of the tank in the form of an anisotropic body is quite approximate and only generally reflects damage to the tank when it is loaded with pressure.

5 Discussion

Before creating the model of the cylindrical tank, the rational parameters tank shell thickness (x_1), honeycomb height (x_2), honeycomb wall thickness (x_3), and honeycomb cell size (x_4) of the cellular system in the interlayer space were determined. The response parameter was chosen to be σei, which occurred on the shell walls at the cross-section.

By modeling the behavior of the tank in the form of a sphere (Figure 1 a), the obtained stress values at the points of the model (Figure 6 a–c) made it possible to build stress distribution diagrams along the wall section (Figure 6 d).

It becomes obvious that under pressure destruction on the inner wall of the tank p_b = 5.0 MPa σ_{ei_max} = 27.5 MPa, i. e., the stresses begin to approach the critical values to the extruded material.

As a result of the model experiments, it was decided to use the following geometric parameters of the cellular tank system: shell thickness h1=2.5 mm, honeycomb height Hs=6.0 mm, honeycomb wall thickness t=2.0 mm, honeycomb cell size K=10 mm, film thickness δp=0.15 mm. The ease of printing and FDM printers also provided such parameters.

Self-fastening of individual shell parts did not significantly change the intensity of stresses, slightly increasing their values, but with a measurement error (about 16 %).

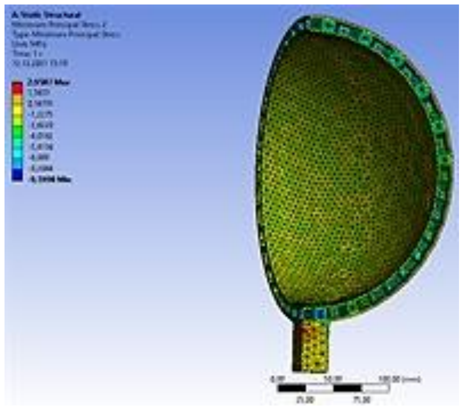

a

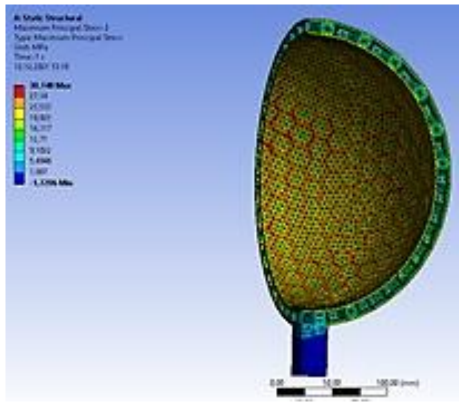

b

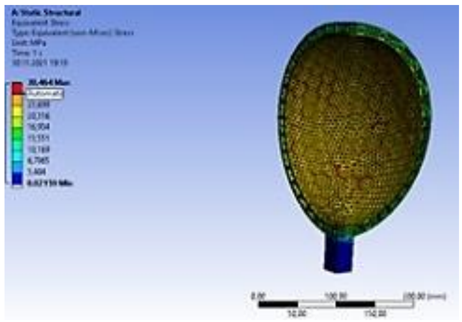

c

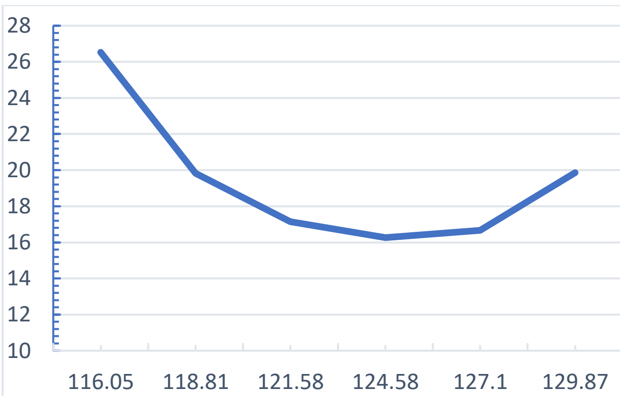

d

Figure 6 – Distribution of normal (a), tangential (b), and equivalent (c) stresses in the spherical shell and the radial direction through the honeycomb wall (d)

The results of experimental tests of demonstrator tanks given in work [21] made it possible to verify the simulation results.

The stress intensity values for testing the material and its modeling differ (about 1.6 %). A practically similar conclusion was made afterward. However, when determining the stress parameters for the tank demonstrator and during simulation, the difference in values was much higher (more than 10%), which can be explained by the fact that a printer with manual adjustment was used to manufacture the demonstrators, therefore, the optimal conditions for laying out the material were achieved was not.

The simulation determined the crack to be formed in a homogeneous material with a $2b = 5.0$ mm size. However, the cracks in the finished products developed less actively, and this can be explained by the fact that the cracks, having formed on the initial defects or cavities, cannot actively develop outside the zone of the next cavity. Their localization helps to increase the crack resistance of the tanks compared to the filament material.

In addition, the mechanical tests given in [22] showed a significant difference in the strength of the products obtained when laying on a flat table and a cylindrical surface. More significant strength indicators were achieved when the filament melt was placed on a cylindrical table when $\sigma_{b\_max\_PC} = 58.5$ MPa, ($[\sigma]_{PC} = 60$–62 MPa – values obtained for the RS material in the form of a filament). Laying out on a flat table made it possible to obtain significantly lower strength: $\sigma_{b\_max\_PC} = 53.5$ MPa. Generally, the given practical results satisfactorily agreed with those predicted for the test sample.

It becomes evident that along with the satisfactory provision of shape and strength parameters under certain types of loads, the methods of predicting the crack resistance of the product and its behavior under the influence of critical loads require significant refinement.

6 Conclusions

This research contributes valuable insights into the additive synthesis of structural components, mainly focusing on the FDM process. Several key conclusions can be drawn through theoretical modeling and finite element analysis.

First, through advanced numerical simulations, the study reveals that increasing internal pressure leads to stresses on inner tank walls nearing 27.5 MPa. This underscores the importance of meticulously considering material properties during the design phase to ensure structural integrity under varying conditions.

Second, the research reveals that damage and destruction in these structures occur progressively, with the central section of the product experiencing the most significant deformation and damage. This underscores the need for careful monitoring and quality control during manufacturing.

Moreover, the study indicates that the thickness of tank walls does not significantly impact the damage development mechanism. However, it highlights the importance of selecting rational parameters for the honeycomb system, including shell thickness, honeycomb height, honeycomb wall thickness, and honeycomb cell size, in minimizing stress concentrations and enhancing product integrity.

Finally, including honeycomb structures within the tank design provides enhanced thermal insulation properties. The research demonstrates that this design feature helps localize damage and mitigate the formation of significant trunk cracks, particularly along generative cracks.

Overall, the use of sophisticated numerical simulations and finite element analysis bolsters the reliability of these results. However, it is essential to acknowledge the study’s limitations, particularly in the context of theoretical modeling. Real-world scenarios are inherently complex, and while digital datasets contribute robust insights, experimental validations are crucial to enhance result reliability.

Future research should focus on experimental validations and real-world testing to bridge the gap between theoretical modeling and practical applications. Exploring a broader spectrum of material properties and investigating the influence of diverse manufacturing parameters will contribute to a more holistic understanding of additive manufacturing processes. Additionally, efforts should be directed towards scalability for industrial applications and developing predictive models for defect mechanisms.

In conclusion, this study provides valuable insights into the intricacies of additive manufacturing and lays the groundwork for future investigations. The continual refinement of our understanding and experimental validations will pave the way for developing more resilient and reliable structural designs in additive manufacturing.

Acknowledgment

The team of authors expresses their deep gratitude to the staff and management of the State Enterprise “Pivdenne Design Office”, E. O. Paton Electric Welding Institute, and National Aerospace University “Kharkiv Aviation Institute” for material support during the preparation and implementation of experiments for assistance in organizing and carrying out work on the study of new materials and products of aerospace technology.

References

1. Vaezi, M., Seitz, H., Yang, S. (2013). A review on 3D micro-additive manufacturing technologies. *The International Journal of Advanced Manufacturing Technology*, Vol. 67(5-8), pp. 1721–1754. https://doi.org/10.1007/s00170-012-4605-2
2. Litot, O., Man'ko, T. (2020). Methods of graphic construction of the process of manufacturing the power shell of composite fuel tanks. *Journal of Rocket and Space Technology*, Vol. 28 (4), pp. 75–81. https://doi.org/10.15421/452010
3. Kumar, S.A., Prasad, R.V.S. (2021). Chapter 2 - Basic principles of additive manufacturing: different additive manufacturing technologies. *Additive Manufacturing*, Vol. 2021, pp. 17–35. https://doi.org/10.1016/B978-0-12-822056-6.00012-6
4. Cano-Vicent, A., Tambuwala, M.M., Hassan, S.S., Barh, D., Aljabali, A.A.A., Birkett, M., Arjunan, A., Serrano-Aroca, A. (2021). Fused deposition modelling: Current status, methodology, applications and future prospects. *Additive Manufacturing*, Vol. 47, 102378. https://doi.org/10.1016/j.addma.2021.102378
5. Cevik, U., Kam, M. (2020). A review study on mechanical properties of obtained products by FDM method and metal/polymer composite filament production. *Journal of Nanomaterials*, Vol. 2020, 6187149. https://doi.org/10.1155/2020/6187149
6. Syrlybayev, D., Zharylkassyn, B., Seisekulova, A., Akhmetov, M., Perveen, A., Talamona, D. (2021). Optimisation of strength properties of FDM printed parts – A critical review. *Polymers*, Vol. 13(10), 1587. https://doi.org/10.3390/polym13101587
7. Garg, A., Bhattacharya, A. (2017). An insight to the failure of FDM parts under tensile loading: finite element analysis and experimental study. *International Journal of Mechanical Sciences*, Vol. 120, pp. 225–236. https://doi.org/10.1016/j.ijmecsci.2016.11.032
8. Torrado, A.R., Roberson, D.A. (2016). Failure analysis and anisotropy evaluation of 3D-printed tensile test specimens of different geometries and print raster patterns. *J Fail. Anal. and Preven*. Vol. 16, pp. 154–164. doi: https://doi.org/10.1007/s11668-016-0067-4
9. Bukkapatnam, S., Clark, B. (2007). Dynamic modeling and monitoring of contour crafting – An extrusion-based layered manufacturing process. *J. Manuf. Sci. Eng*, Vol. 129(1), pp. 135–142. https://doi.org/10.1115/1.2375137
10. Caminero, M.A., Chacón, J.M., García-Moreno, I., Rodríguez, G.P. (2018). Impact damage resistance of 3D printed continuous fibre reinforced thermoplastic composites using fused deposition modeling. *Composites Part B: Engineering*, Vol. 148, pp. 93–103. https://doi.org/10.1016/j.compositesb.2018.04.054
11. Park, S., Watanabe, N., Rosen, D.W. (2018). Estimating failure of material extrusion truss structures based on deposition modeling and a cohesive zone model. *Materials & Design*, Vol. 147, pp. 122–133. https://doi.org/10.1016/j.matdes.2018.03.034
12. Shanmugam, V., Rajendran, D.J.J., Babu, K., Rajendran, S., Veerasimman, A., Marimuthu, U., Singh, S., Das, O., Neisiany, R.E., Hedenqvist, M.S., Berto, F., Ramakrishna, S. (2021). The mechanical testing and performance analysis of polymer-fibre composites prepared through the additive manufacturing. *Polymer Testing*, Vol. 93, 106925. https://doi.org/10.1016/j.polymertesting.2020.106925
13. Avramov, K., Uspensky, B. (2023). Nonlinear vibrations of doubly curved composite sandwich shells with FDM additively manufactured flexible honeycomb core. *Acta Mech*, Vol. 234, pp. 1183–1210. https://doi.org/10.1007/s00707-022-03426-w
14. Avramov, K.V., Uspenskyi, B.V., Urniaieva, I.A., Breslavskyi, I.D. (2023). Bifurcations and stability of nonlinear vibrations of a three-layer composite shell with moderate amplitudes. *Journal of Mechanical Engineering*, Vol. 26 (2), pp. 6–15. https://doi.org/10.15407/pmach2023.02.006
15. Salenko, A., Kostenko, A., Tsurkan, D., Zinchuk, A., Zagirnyak, M., Orel, V., Arhat, R., Derevianko, I., Samusenko, A. (2023). A new FDM printer concept for printing cylindrical workpieces. In: *Information Technology for Education, Science, and Technics. ITEST 2022. Lecture Notes on Data Engineering and Communications Technologies*, Vol. 178, pp. 459–483. Springer, Cham. https://doi.org/10.1007/978-3-031-35467-0_28
16. Das, P., Islam, M.A., Somadder, S., Hasib, M.A. (2022). Analytical and numerical analysis of functionally graded (FGM) axisymmetric cylinders under thermo-mechanical loadings. *Materials Today Communications*, Vol. 33, pp. 104405. doi: https://doi.org/10.1016/j.mtcomm.2022.104405
17. Litot, A., Man'ko, T. (2020). Modeling of a multilayer composite material of a fuel tank flange from CFRP. *System Technologies*, Vol. 6(131), pp. 3–9. https://doi.org/10.34185/1562-9945-6-131-2020-01
18. Lawrence, W., Fisher, P.E. (2005). *Selection of Engineering Materials and Adhesives*. CRC Press – Taylor & Francis Group, Boca Raton, FL, USA.
19. Khaleelullah, A., Basha, S.J., Rangavittal, H.K. (2012). Design and analysis of propellant tanks support structure for an advanced spacecraft. *International Journal of Applied Research in Mechanical Engineering*, Vol. 1(2), pp. 75–81. https://doi.org/10.47893/IJARME.2012.1035
20. Salenko, O., Zagirnyak, M., Orel, V., Shlyk, S., Kulynych, V. (2022). FDM products strength increasing using the algorithmic means of 3-D printers working. In: *2022 IEEE 4th International Conference on Modern Electrical and Energy System (MEES)*, pp. 1–5. https://doi.org/10.1109/MEES58014.2022.10005667
21. Salenko, O., Dzhulii, D., Drahobetskyi, V., Symonova, A., Moloshtan, D. (2023). Damage mechanisms of multilayer axisymmetric shells obtained by the FDM method. In: *Advances in Design, Simulation and Manufacturing VI. DSMIE 2023. Lecture Notes in Mechanical Engineering*, pp. 270–281. Springer, Cham. https://doi.org/10.1007/978-3-031-32774-2_27
22. Tichý, T., Šefl, O., Veselý, P., Dušek, K., Bušek, D. (2021). Mathematical modelling of temperature distribution in selected parts of FFF printer during 3D printing process. *Polymers*, Vol. 13(23), 4213. https://doi.org/10.3390/polym13234213